NOTICE
This report was prepared as an account of work sponsored by the United States Government. Neither the United States nor the United States Energy Research and Development Administration, nor any of their employees, nor any of their contractors, subcontractors, or their employees, makes any warranty, express or implied, or assumes any legal liability or responsibility for the accuracy, completeness or usefulness of any information, apparatus, product or process disclosed, or represents that its use would not infringe privately owned rights.

MULTIPLICITY AND CHARGED PARTICLE EMISSION IN RELATIVISTIC HEAVY ION COLLISIONS[1])

H. H. Gutbrod, J. Gosset, W. G. Meyer, A. M. Poskanzer, A. Sandoval, R. Stock, and G. D. Westfall

Lawrence Berkeley Laboratory, Berkeley, CA 94720
Gesellschaft für Schwerionenforschung, Darmstadt, Germany
Fachbereich Physik, Universität Marburg, Marburg, Germany

The π^- data were taken by S. Nagamiya et al.[2]) and we are grateful to the authors to allow us to present them here.

I. Introduction

After nearly three years of Bevalac research, the interest has shifted from the peripheral reactions--studied intensively by the Heckman/Greiner group and described successfully by the abrasion-ablation model[7])--to near central collisions. Whereas peripheral reactions proceed with relatively small transfer of momentum and energy, the near-central collision is characterized at high incident energies with an almost complete dissociation of both target and projectile, as made visible in some streamer chamber pictures[3]).

It has been generally accepted that a high multiplicity of fragments and pions at large angles and intermediate energies may be used as a distinctive feature that allows one to select near central collisions of relativistic nuclei. Since many motivations for the relativistic heavy ion physics have and will be given by the theorists present at this conference we can cut this introduction short and focus immediately onto experimental facts and observations[1]) available now after about two years of central collision studies at the Bevalac. We will have to leave the beautiful "star-observations" to the next two speakers and will concentrate onto single particle inclusive cross sections of precisely identified fragments (as to their charge, mass, energy, and emission angle) together with associated multiplicities of fast charged particles.

We will see that all the observed fragment spectra are structureless and more or less exponentially decaying throughout the range of studied fragment masses. We will give a catalogue of experimentally found qualitative features and will look then into the applicability of simple statistical thermodynamic models by tracing down in the spectra kinematical effects in the framework of a source of a temperature T

DISTRIBUTION OF THIS DOCUMENT IS UNLIMITED

MASTER

and a velocity β. This leads directly to the "nuclear fireball-model"[4]) we presented nearly a year ago.

The production of complex particles will be discussed next. A simple mass dependence in the cross section of the fragments is observed[5]) and leads us to the question if a stuck projectile and the explosion of a "compound nucleus" would make any sense.

II. Experimental Techniques

The basic layout of the experimental setup consisted of a particle telescope mounted on a movable arm inside a scattering chamber, a monitor telescope fixed at 90°, used to obtain the relative normalization, and an array of fifteen plastic scintillator paddles (tag counters) placed outside the scattering chamber, subtending the angles between 15° and 60° with respect to the beam direction, and about one-third of the azimuth. This array was used to determine the multiplicity of charged particles, with energies above ∿50 MeV/nucleon, associated with each event measured in the telescope.

Several different telescopes have been used to measure the large spectrum of masses and energies in this experiment. Evaporation-like fragments were detected in thin ΔE-E silicon detector telescopes with thicknesses of 22 μm, 205 μm, and 177 μm and 1500 μm. The high energy components of helium and hydrogen isotopes were measured with a ΔE-E telescope consisting of a 2 mm ΔE-silicon detector and a 10 cm, conically shaped scintillator coupled to a 2.5 cm phototube as an E detector.

The yields of the elements between lithium and oxygen above an energy of about 100 MeV were measured with a three element telescope, Fig. 1, consisting of a large area of thin Si ΔE detectors (180 μm) followed by the same area of 3 mm thick intrinsic germanium which was followed by the 3rd element an 8 mm intrinsic germanium detector. This ΔE_1-ΔE_2-E telescope was in the Si elements subgrouped into six angular bins so that six angular steps could be measured simultaneously. Particle identifier spectra of these telescopes are shown in Fig. 2. As a result of the quality of these detectors, we can give the precise mass, charge, and

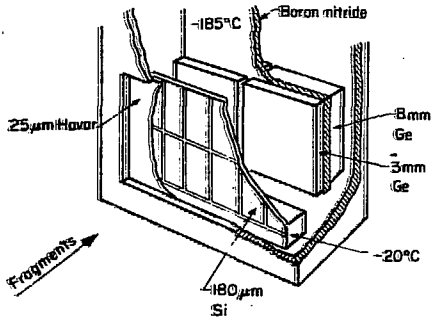

Fig. 1 xBL 773-595

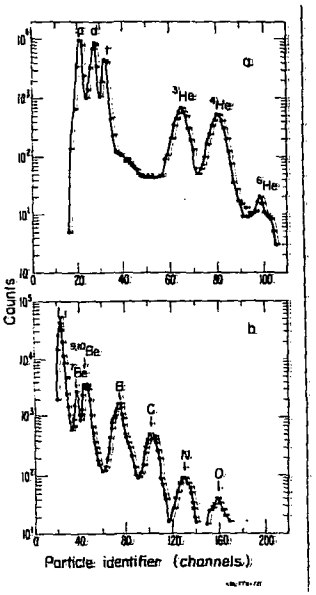

Fig. 2

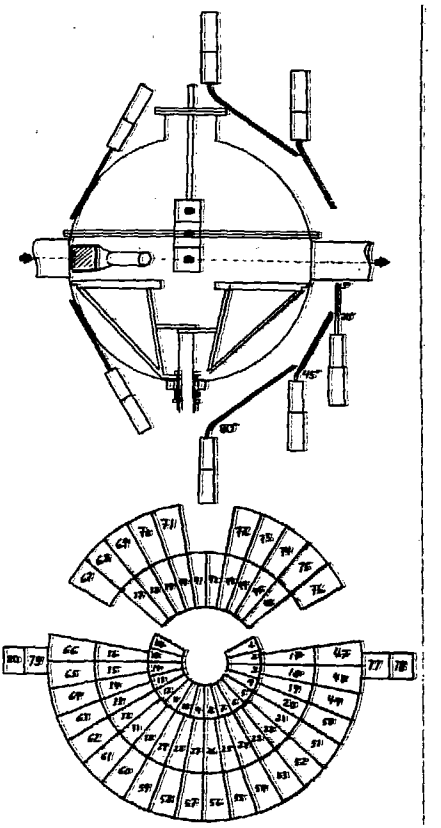

Fig. 3

energy as well as the reaction angle of the detected particles up to ^{4}He. From Li on we have isotope resolution only where indicated in the figures.

We have recently improved our setup by placing 80 photomultipliers with scintillators around a thin spherical scattering chamber, Fig. 3, which allows us to recognize much better the pattern of the star-event. The lower part of the figure shows the multiplicity-ring pattern looking in beam direction. Also in this new setup, we do exclude from the measured multiplicity all particles below an energy of 25 MeV/n. Thus we are sure not to measure low evaporation like fragments in the associated multiplicity. Furthermore we built a new telescope capable of detecting π^+ from 17 to 100 MeV and protons from 5 to 200 MeV etc. Some of the data I show are already from this vintage. The π^- distributions are taken from ref. [2]) and were measured in a magnetic spectrometer.

III. Experimental Results

Let us have first a look at the low-energy or evaporation like fragments. Figure 4 shows the 90° energy spectra of He to Be isotopes in the low energy region for ^{20}Ne bombardment of U at 2.1 GeV/nucleon. These energy spectra show a Maxwellian shape with the peak position shifting towards higher energies as the atomic number of the fragment increases. For a given element, the most neutron deficient isotope displays a more prominent high energy component. This trend is most obvious in Fig. 4 for ^{6}Li and ^{7}Be. It is also observed for the He isotopes as will be indicated below.

The cross section for the evaporation like α-particle is so high that—from an estimate of the integrated low energy α-particle yield—on the average about 7 α-particles are emitted per interaction. These low energy particles are not included in the later discussed associated multiplicities.

At high fragment energies the double differential cross sections for ^{20}Ne on U at 400 MeV/nucleon as an example presented in Fig. 5 are smooth and exponentially decaying with increasing energy, being flattest for the protons and becoming steeper as the mass of the fragment increases. For a given fragment the slope of the energy spectra rapidly increases with increasing angle, and the yield of each fragment decreases as the mass or charge of the fragment increases. A deviation from this general trend is

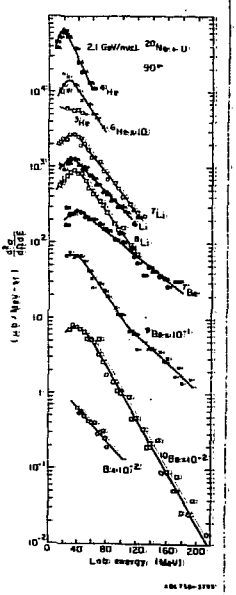

Fig. 4

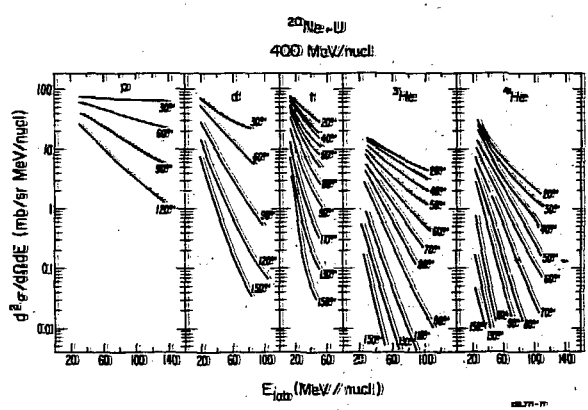

Fig. 5

observed in the vicinity of the evaporation region where the yield is higher for ^{4}He than for ^{3}He. In turn, ^{3}He exhibits a relatively more prominent high energy cross section. In this respect, the He isotope cross sections follow the trend of neutron deficient isotope cross sections, as described earlier.

The proton energy spectra from ^{20}Ne n U at forward angles are extremely flat in the measured energy range. It is surprising to find that the usual kinematical argument that would predict more forward peaked angular distributions the higher the combarding energy does not apply. In fact the trend is opposite for all the fragments as shown in Fig. 6 in the angular distributions labeled a, b, c, which are ^{3}He fragments integrated in the indicated energy windows from Ne on U at 2100, 400, 250 MeV/nucleon respectively. At the highest bombarding energy the cross section changes by less than an order of magnitude from 20 to 130 degrees, while for the 250 MeV/nucleon bombarding energy it changes by more than two orders of magnitude. Similar ^{3}He angular distributions are observed in the energy window from 50 to 100 MeV/nucleon. The overall features are the same but all slopes are steeper. A comparison at 2100 MeV/nucleon between (a) uranium and (b) Al as target shows that for light targets the backward hemisphere is depleted. At 400 MeV/nucleon incident (e) ^{4}He and (b) ^{20}Ne on uranium there is no significant difference in the shape of the angular distributions. Note that curves (d) and (e) are raised in absolute value by a factor of 10 for better graphical representation.

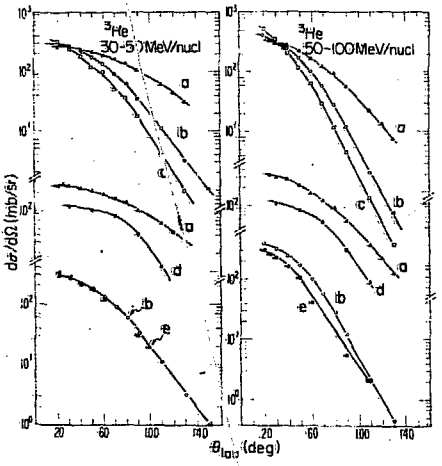

Fig. 6

In general for fixed target, projectile, and incident energy, the angular distributions of all fragments become more forward peaked the higher the energy window considered. Therefore, the value of angular distributions of integrated spectra in these experiments is small and the presentation of double differential cross sections should be preferred.

Looking now at the heavier fragments at intermediate energies in Fig. 7, the slopes of the spectra also get steeper with increase in reaction angle

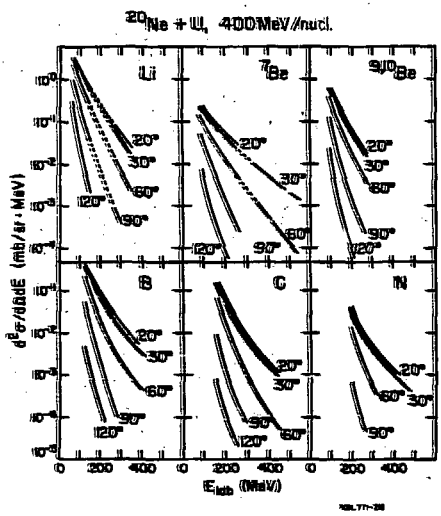

Fig. 7

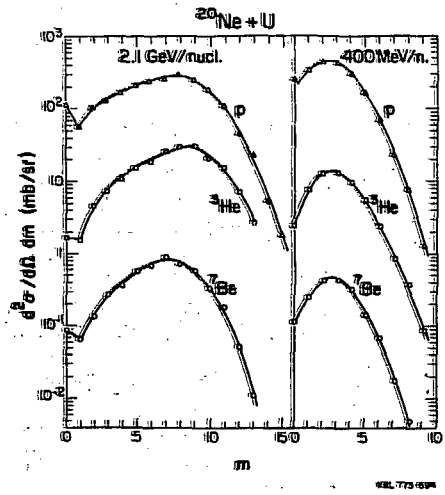

Fig. 8

for a fixed fragment. The changes of the slopes with fragment mass at a given angle are less pronounced than before, but note that here the spectra are plotted in MeV instead of MeV/nucleon as in the case of hydrogen and helium isotopes previously shown.

The associated multiplicities should give us a hint whether we are indeed observing near central collisions. Figure 8 shows from the 15 tag counter array m-fold coincidence cross sections associated with three different fragments detected in the telescope at 90°. For all fragments the average multiplicity is large reflecting quite a large transverse momentum transfer since the tag array is sensitive to particles like protons above 50 MeV. In the new experimental set-up the selection of various multiplicity patterns is possible.

In Fig. 9(a) the paddle histogram is shown on the top associated with Si-Ge telescope events on the bottom associated with the monitor telescope. Monitor telescope and Si-Ge telescope are placed opposite of each other at 90°. We observe clearly in ring A and B a large angle--two particle--correlation between fragments in the telescope and fragments in the paddles enhancing the yield in the forward angles opposite to

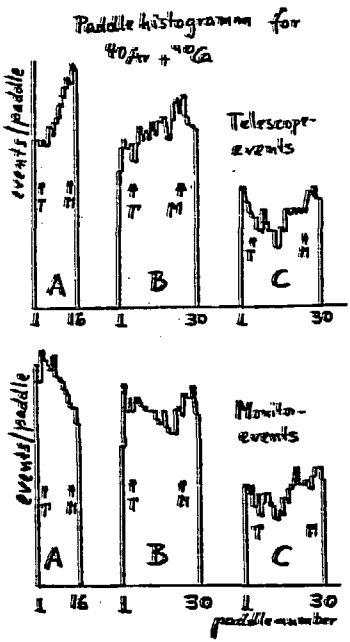

Fig. 9 (a)

the detected fragment. Note that we are looking here at star events with average total multiplicities of at least 12 high energy particles in the 9°-80° forward hemisphere. We are presently studying this correlation as a function of angle θ of the telescope and fragment energy. Figure 9(b) shows the difference in the paddle histogram for ^{40}Ar on Ca and U. For ^{40}Ar on Ca the prongs are much more forward peaked than for U.

In order to ease the discussion the main characteristic features of the data may be summarized in the following way:

Summary of Qualitative Features of the Data

1) All light fragment energy spectra are smooth except for an "evaporation peak" at very low energies.
2) The most neutron deficient isotopes exhibit spectra with

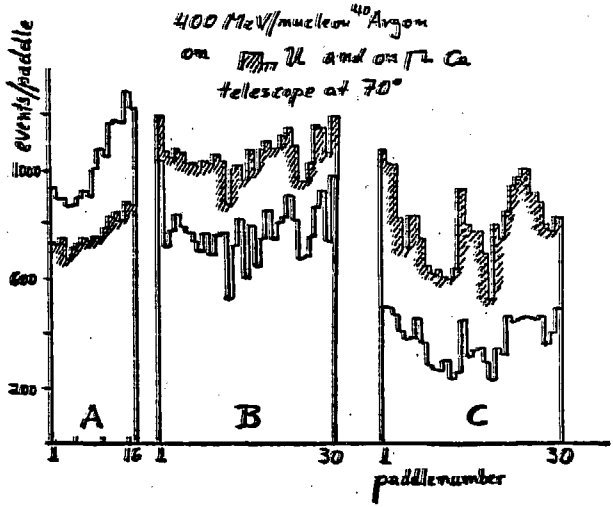

Fig. 9 (b)

a relatively higher cross section in the high energy tail.
3) The slope of the fragment spectra in the intermediate energy range gets steeper with increasing detection angle. Angular distributions are forward peaked.
4) The double differential cross sections for Ne on U at 30° are approximately independent of the incident energy for a given fragment. At larger angles the yield increases and the slope decreases with increasing bombarding energy.
5) The slope of the fragment spectra in energy/nucleon at a given angle gets steeper with increase in fragment mass.
6) The total yields of light fragments fall off with increase in mass. At energies of 30-50 MeV/nucleon cluster emission comprises a significant fraction (about 50%) of the total baryonic cross section. Towards higher energies protons become predominant.
7) Increasing the projectile mass at a fixed incident energy per nucleon leads to a small increase in the cross section for low energy fragments but to a larger increase at high fragment energies, especially for the heavier clusters.
8) In Ne and Ar bombardment of U, Ca, and Al targets besides the difference in overall absolute cross section, one finds for Ca and Al a depletion of cross section at back angles.
9) For all particles detected at angles between 20° and 160° the mean associated multiplicity is high and not changing remarkably with fragment mass or energy.
10) The mean associated multiplicity increases with the projectile mass and with the target mass.
11) Large angle emission of energetic fragments is enhanced in high multiplicity events.

IV. Discussion of the Data

In the peripheral reactions it is rather easy to determine where the particles originated by just looking at around 0° and at a fragment velocity equivalent to that of the projectile. Here, however, we cover a large spectrum of longitudinal velocities and need therefore an appropriate representation of the longitudinal and transverse momenta of the fragments.

In Figs. 10 and 11 contours of constant invariant cross sections $\frac{1}{p}\frac{d^2\sigma}{dEd\Omega}$ are given in a $(y,p_\perp)$ plane for different fragments from ^{20}Ne on U at 400 MeV/nucleon and for ^{3}He fragments from ^{20}Ne on U at different bombarding energies. y is the rapidity of the fragment defined as

$$y = \frac{1}{2}\ln[(E+p_\parallel)/(E-p_\parallel)].$$

This variable is simply shifted by a constant value if

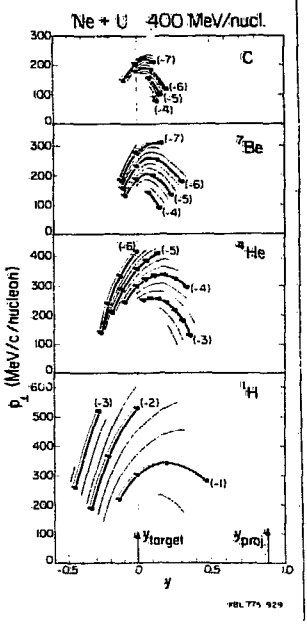

Fig. 10

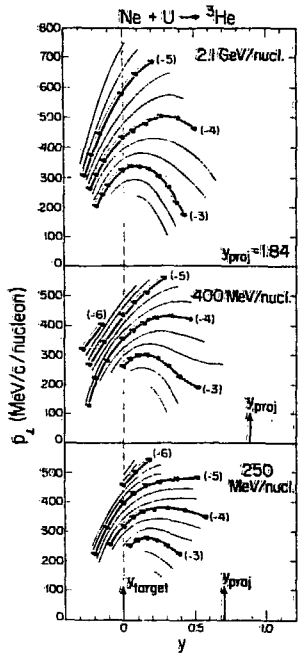

Fig. 11

expressed in a moving frame. y is approximately equal to β for small velocities. $p_\perp$ is the transverse momentum per nucleon of a fragment. In the contours the spacing between the lines corresponds to a constant factor in cross section. The thick lines are labelled by the common logarithm of the invariant cross sections. Such contour plots are invariant with respect to Lorentz transformations, except for a shift of the rapidity axis.

In these contour plots the maximum $p_\perp$ on a given contour line lies at a value of y which can be attributed to the velocity of an apparent source. In Fig. 10 it is clear that at low $p_\perp$ values the apparent source velocities are close to zero but that as we go up in $p_\perp$ the associated y goes up too. (Note that we plot here $p_\perp$/nucleon.) Thus it is clear that these fragments are not emitted isotropically from one unique moving source, which would give contour lines all centered around the rapidity of that source. In a peripheral collision the fragments from target and projectile would be

represented by two steep "mountains" symmetric about the target and projectile rapidities. It is obvious that the present data do not cover the region of projectile fragmentation. Target fragmentation products may be part of the cross section only for the lowest values of $p_\perp$ and y. Most of our data thus represent fragments from non-peripheral collisions.

The maximum of the invariant cross section at a given level of $p_\perp$ occurs at increasing values of the rapidity for increasing $p_\perp$. Due to the shift of the contour lines towards intermediate rapidities with wider spacing, there is clear indication for at least two qualitatively different sources

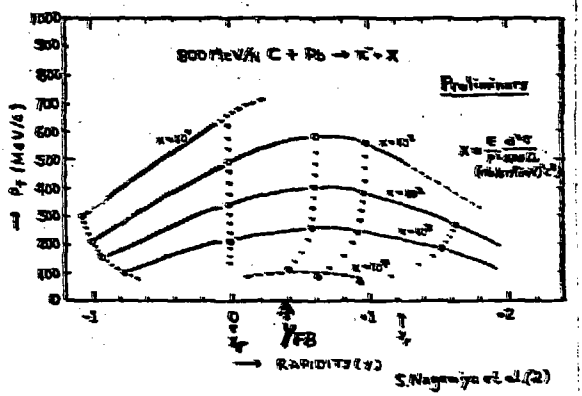

Fig. 12

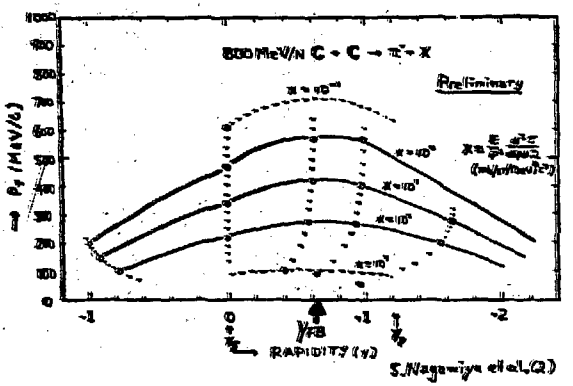

participating in the fragment emission. One source is moving slowly in the lab with a rapidity smaller than about 0.1. It accounts for the emission both of protons and clusters at small transverse momenta, $p_\perp$/nucleon $\leq$250 MeV/c (explosion of the total target and projectile system and/or target spectator decay). The other source moves with a rapidity intermediate between those of the target and projectile, and its decay products extend towards higher transverse momenta, corresponding to the highest energy and momentum transfer between the target and the projectile.

Before we go to the fireball model which tries to reproduce these findings, I show you again a $(y,p_\perp)$ contour plot, Fig. 12, this time for π^- emitted from 800 MeV/nucleon C on C and U, measured by S. Nagamiya, et al. The picture here is totally different from that just seen. There is no difference between C and C--which is in a kinematical point of view a nucleon-nucleon system--and C on Pb. Therefore one is led to conclude that the source of pions at these transverse momenta is purely of nucleon-nucleon nature and does not reflect any collective effects, in contrast to that of the charged particle distributions which cannot be described with one single longitudinal source velocity.

V. Fireball and Coalescence

The change in slope of the spectra as a function of angle gave a clear hint to try a thermodynamic model based on a moving source with velocity β and temperature τ. Since the observed rapidities were much higher than that of the center of mass of projectile and target, subsystems had to be found with higher apparent velocity. This led directly to the nuclear fireball model presented nearly a year ago[4]), which will be outlined shortly in the following:

When a relativistic heavy ion projectile collides with a target nucleus there should be during a primary fast stage a localization of the interaction to the overlapping domain of target and projectile densities while the rest of the two nuclei remain relatively undisturbed. On a secondary time scale, dissipation of compressional and surface energy, as well as reabsorption of pions and nucleons emitted from the primary interaction region will excite these remnants, resulting in their subsequent decay that should be characterized by moderately low energies. This idea leads to the separation of the nucleons in the system into participants and spectators with respect to the time scale of the fast interaction stage. The nuclear fireball model deals only with the participant nucleons, i.e., it refers to a sub-set of the emitted particles. The model assumes that the two nuclei sweep out cylindrical cuts through each other, Fig. 13.

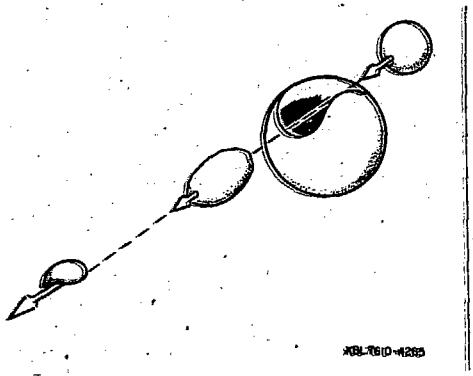

Fig. 13

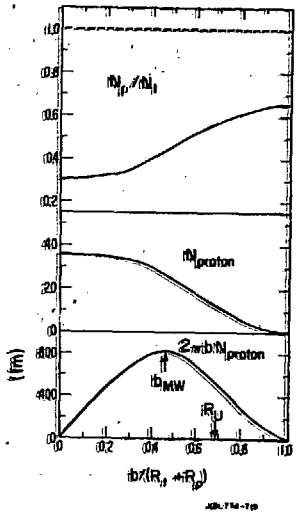

Fig. 14

The projectile participants are assumed to transfer all of their momentum to the effective center of mass system of all the participant nucleons forming a fireball which moves forward in the lab at a velocity intermediate between those of target and projectile. Its average internal kinetic energy per nucleon is much higher than the binding energy per nucleon. The participant nucleon fireball is then treated as an equilibrated non-rotating ideal gas characterized by a temperature, which expands isotropically in the center of mass of the fireball with a Maxwellian distribution in energy. The number of participants is calculated for each impact parameter. For nonsymmetric systems the effective center of mass of the participants is impact parameter dependent as is the fireball temperature. Only for symmetric systems like ^{40}Ar on ^{40}Ca exists a unique $\beta_{fireball}$ and $T_{fireball}$. Figure 14 shows the geometrical quantities as a function of impact parameter. N_p/N_t is the ratio of projectile to target participant nucleons, N_{proton} is the number of participant protons, and $2\pi b N_{proton}$ is the weight given to each impact parameter. The solid lines represent the case of Ne on U and the dashed line an equal mass projectile-target combination. The arrow on the abscissa indicates the radius of uranium and the arrow labeled b_{MW} indicates the impact parameter with the maximum weight.

Figure 15 shows kinematical quantities as a function of impact parameter calculated in the fireball model. The velocity of the fireball in the lab is β and ε is the available kinetic energy per nucleon in the fireball. The comparison of the data with that model, integrated over all

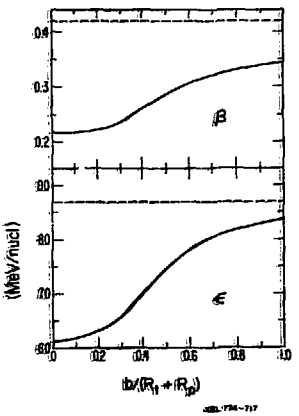

← Fig. 15

Fig. 16 →

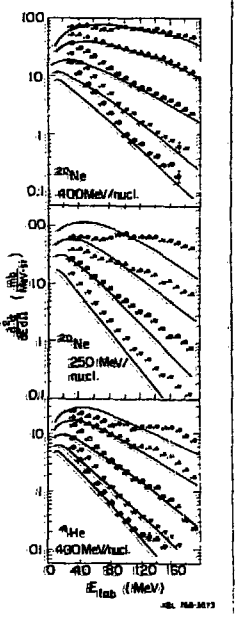

impact parameters, is shown in Fig. 16 for ^{20}Ne+U at 400 MeV/nucleon, 250 MeV/nucleon and for ^{4}He+U at 400 MeV/nucleon.

Going back to Figs. 10 and 11 for 400 MeV/nucleon ^{20}Ne+U, the fireball rapidity is 0.28 for the most probable weight and fits well with simply extracted values of y for high $p_\perp$ values. For the π^- data in Fig. 12 we see that the fireball rapidity for C+Pb is totally off from the extracted value of 0.6, equivalent to that in C+C.

Contemplating over such a simple model one often questions first the assumption of clear cylindrical cuts. Shooting holes into nuclei does not sound reasonable in the face of nucleon mean-free-path arguments. Yet, a single molecule hitting a thick wooden plate with a velocity of 1 km/sec has no chance to go through, but if this molecule travels as part of a bullet it easily can make it to the other side. From this viewpoint the nuclear fireball model should be more successful the heavier the projectile mass is. Surprisingly, however, the model can even describe double differential spectra of protons from p on Bi at 450 MeV.

The presented fireball model has been extended to include complex particle production[6-9]. This will raise the temperature in the fireball, since in the chemical equilibrium fewer degrees of freedom are available if clusters do exist. Our data do indicate (see Figs. 10 and 11) that the low $p_\perp$ fragments do come from slow moving sources with velocities from

that of the target-projectile center-of-mass down to zero. If one looks at boron (Fig. 17) then a two parameter fit of a moving source with a velocity $\beta = 0.6$ and a temperature $\tau = 27$ MeV yields fair agreement with the data. This velocity and temperature combination, however, is close to that of a formed compound system, i.e., the projectile gets stuck in the target nucleus and randomizes totally its energy. If such a picture would be true the tremendous angular momenta in that system (nearly 500ħ for Ne+U at 400 MeV/nucleon) would change the decay pattern of the fragments and lower the temperature due to the rotational energy.

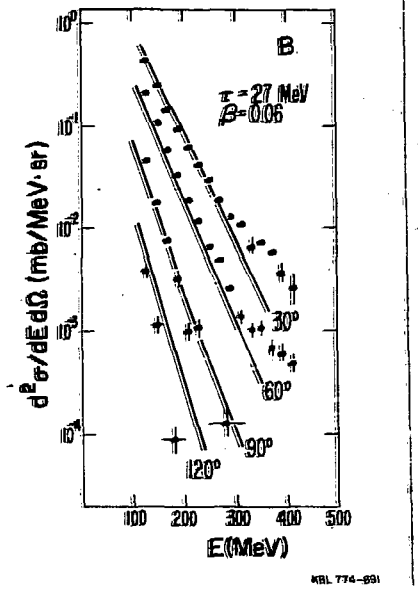

Fig. 17

If one assumes that protons at a given momentum are produced by the same mechanism as the heavier fragments at the same momentum/nucleon then one can, as we did[5]), try to express the complex particles in terms of nucleon double differential cross sections.

Our first attempt to explain the emission of high energy light nuclei in relativistic heavy ion collisions was by final state interactions, or coalescence of emitted nucleons. In this model, if any number of protons and neutrons corresponding to a bound nucleus are emitted in a reaction with momenta differing by less than a coalescence radius p_o, these nucleons are assumed to coalesce and form a nucleus. The cross sections for the emission of light nuclei are then simply related to the cross sections for the emission of nucleons at the same momentum per nucleon, namely,

$$\frac{d^2\sigma_A}{p^2 dp d\Omega} = \frac{1}{A!}\left(\frac{4\pi\ p_o^3\ \gamma}{3\sigma_o}\right)^{A-1}\left(\frac{d^2\sigma_1}{p^2 dp d\Omega}\right)^A .$$

Both cross sections σ_A, for emission of a light nucleus formed with A nucleons, and σ_1, for emission of a single nucleon, are evaluated at the same momentum per nucleon p with Lorentz

factor γ, and σ_0 is the total reaction cross section. Our proton data have been used to calculate the light fragment cross sections from this eugation; the results have been compared with our experimental data, the only adjustable parameter being p_0. In Fig. 18 such a comparison is shown for d, t, ^{3}He, and ^{4}He from the reactions of Ne on U at 250 and 400 MeV/nucleon. The agreement between this simple calculation and our data is rather impressive, the largest discrepancy being for ^{3}He fragments at the lowest energies and at forward angles. The values of the parameter p_0 are remarkably uniform and of reasonable magnitude, between 126 and 147 MeV/c, since they are smaller than the Fermi momenta of the clusters. It should be noticed that this simple phase space calculation does not explicitly include many factors, like spin and isospin couplings, integration over configuration space (not only momentum space) and time. All these factors are hidden in the p_0 value. In Fig. 19 it is shown that a similar calculation leads to a similar agreement with our data for heavier fragments, namely the lithium isotopes (our data include all isotopes, but the calculation has been done assuming mass 6) and ^{7}Be, with a p_0 of the same order of magnitude as that found from the light fragments. For the heaviest fragments, $^{9\to10}$Be to O, the overlap between the energy per nucleon

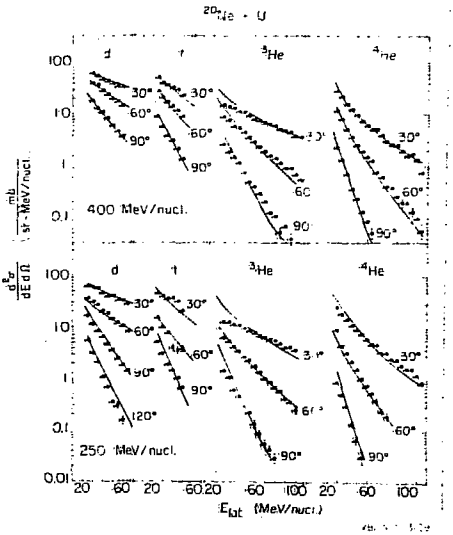

Fig. 18

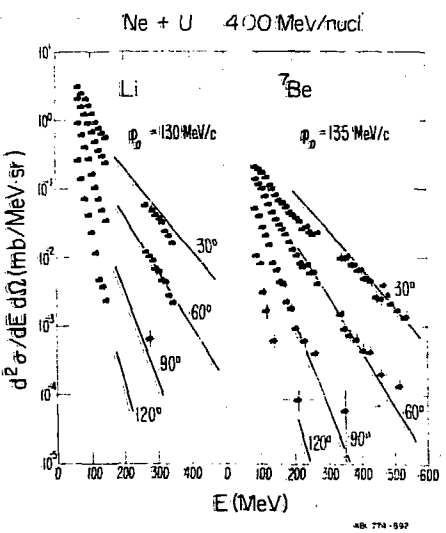

Fig. 19

range of these data and the range of our proton data is too small to make useful comparisons.

The success of the coalescence model, however, has to be looked at as a first glance into the mass dependence of the fragment distribution. The correct treatment of a final state interaction model has to start with a primary nucleon distribution which is different from our procedure. In fact if one guesses such a primary proton distribution one gets smaller values of p_0 and destroys the simple dependence of light nuclei cross sections on nucleon cross sections.

It is very interesting to note that the observed power-law between proton- and cluster cross sections is valid in a thermodynamical picture like that of the fireball. There, the double differential cross section in momentum space for emitting any cluster consisting of A nucleons decreases exponentially with the total kinetic energy E of the cluster like $\exp(-E/\tau)$ where τ is the temperature. Hence with respect to the kinetic energy per nucleon E/A it behaves like $(\exp - \frac{E/A}{\tau})^A$ which is proportional to the Ath power of the cross section for emitting a single nucleon at this energy per nucleon E/A, in contrast to the coalescence model. In the thermodynamical model we do not have to guess a primary nucleon distribution in momentum space. There is interesting physical information in the thermodynamic model, since the yeilds of different nuclear species measured in relativistic heavy ion collisions can be used to obtain the freeze-out density[6]) of their emitting systems, namely the density below which the hot matter expands freely.

In summary, fragments from near central collisions of relativistic heavy ions may originate from several qualitatively different sybsystems of the overall decaying nuclear system, such as the fireball, the target spectators, or alternatively, an explosion of the fused target-projectile system. There is strong support of the validity of thermodynamical models in the production of all fragments observed and the large amount of theorists in this field is promising exciting insights in the near future. The charged particles seem to have clear fingerprints of a collective reaction mechanism whereas the π^- data observed at high pion energies seems not to be different from nucleon-nucleon collisions.

References

1) J. Gosset, H. H. Gutbrod, W. G. Meyer, A. M. Poskanzer, A. Sandoval, R. Stock, and G. D. Westfall, LBL-5820, 1977, and submitted to Phys. Rev. C.

2) S. Nagamiya, I. Tanihata, S. R. Schnetzer, W. Brückner, L. Anderson, G. Shapiro, H. Steiner, and O. Chamberlain, private communication.

3) R. Poe, S. Fung, B. Gorn, A. Kernan, G. Kiernan, J. Lee, J. Ozawa, B. Shen, G. Van Dalin, L. Schroeder, and H. Steiner, to be published.

4) G. D. Westfall, J. Gosset, P. J. Johansen, A. M. Poskanzer, W. G. Meyer, H. H. Gutbrod, A. Sandoval, and R. Stock, Phys. Rev. Letters 37 (1976) 1202.

5) H. H. Gutbrod, A. Sandoval, P. J. Johansen, A. M. Poskanzer, J. Gosset, W. G. Meyer, G. D. Westfall, and R. Stock, Phys. Rev. Letters 37 (1976) 667; and H. H. Gutbrod, Journal de Physique Colloque C-5 (1976) 209.

6) A. Mekjian, Phys. Rev. Letters 38 (1977) 640; and S. Garpman, J. Bond, and P. J. Johansen, to be published.

7) J. D. Bowman, W. J. Swiatecki, and C. F. Tsang, LBL-2908, unpublished report (1973).

Work performed under the auspices of the U. S. Energy Research and Development Administration.